Research Square

Preprints are preliminary reports that have not undergone peer review.
They should not be considered conclusive, used to inform clinical practice,
or referenced by the media as validated information.

Systematic identification of perioperative neurocognitive disorder related biomarkers in Alzheimer's disease and development of machine learning-based diagnostic models

Zhaoliang Gu
Affiliated Hospital of Qingdao University
Yuan Dong
Affiliated Hospital of Qingdao University
Shipeng Shang
Qingdao University
Aijie Liu
Affiliated Hospital of Qingdao University
Jing Wang
Affiliated Hospital of Qingdao University
Xiaosa Chi
Affiliated Hospital of Qingdao University
Anmu Xie
Affiliated Hospital of Qingdao University
Mingjuan Li
limingjuan@qdu.edu.cn
Affiliated Hospital of Qingdao University

Research Article

Keywords: Perioperative Neurocognitive Disorder, Alzheimer's disease, Biomarkers, Neurodegenerative diseases, Machine learning

Posted Date: October 16th, 2026

DOI: https://doi.org/10.21203/rs.3.rs-8965858/v1

License: This work is licensed under a Creative Commons Attribution 4.0 International License.
Read Full License

Additional Declarations:
No competing interests reported.

Tables 1 is available in the supplementary files section.

Systematic identification of perioperative neurocognitive disorder related biomarkers in Alzheimer's disease and development of machine learning-based diagnostic models

Zhaoliang Gu 1, Yuan Dong 2, Shipeng Shang 5, 6, 7, Aijie Liu 1, Jing Wang 3, Xiaosa Chi 4, Anmu Xie 3, Mingjuan Li 1*

[1] Department of Anesthesiology, the Affiliated Hospital of Qingdao University, Qingdao, China

[2] Neuropsychiatry Research Institute (NPRI), the Affiliated Hospital of Qingdao University, Qingdao, China

[3] Department of Neurology, the Affiliated Hospital of Qingdao University, Qingdao, China

[4] Department of Geriatrics, the Affiliated Hospital of Qingdao University, Qingdao, China

[5] School of Basic Medicine, Qingdao University, Qingdao, China

[6] Clinical Research Center (CRC), Medical Pathology Center (MPC), Cancer Early Detection and Treatment Center (CEDTC), Chongqing University Three Gorges Hospital, Chongqing University, Chongqing, China

[7] Translational Medicine Research Center (TMRC), School of Medicine Chongqing University, Chongqing, China

*Corresponding author: Mingjuan Li

E-mail address: limingjuan@qdu.edu.cn

Keywords: Perioperative Neurocognitive Disorder, Alzheimer's disease, Biomarkers, Neurodegenerative diseases, Machine learning

Abstract

Alzheimer's disease (AD) is a widely prevalent neurodegenerative disorder characterized by progressive cognitive impairment and neuropathological alterations. Accumulating evidence suggests that perioperative neurocognitive disorder (PND) shares several pathological characteristics with AD; however, the molecular crosstalk between these two disorders and relevant biomarkers remain largely unexplored. In this study, we performed an integrated analysis of high-throughput sequencing datasets from Alzheimer's disease cohorts and systematically identified the core regulatory protein-protein interaction (PPI) network associated with AD. Utilizing a random forest machine learning algorithm, we identified 10 potential core biomarkers from this network. Through comprehensive multi-cohort validation analyses, six robust biomarkers RB1, PARK7, GLO1, ENO2, MDH2, and TUBB were ultimately confirmed. In addition, in vivo validation in the 5×FAD mouse model provided experimental support for the overall dysregulation trends of these candidate biomarkers. Based on these six conserved biomarkers, we developed a diagnostic nomogram model for molecular classification and clinical assessment of Alzheimer's disease. Functional enrichment analyses demonstrated significant associations between these biomarkers and conserved immune-related and metabolic pathways in AD. Furthermore, immune infiltration analysis revealed correlations between identified genes and multiple immune cell subtypes, suggesting immune modulation as a critical shared mechanism. Finally, we constructed a drug-target interaction network based on these biomarkers, providing valuable insights into potential therapeutic targets for the treatment of both PND and AD.

1. **Introduction**

Alzheimer's disease (AD) is a progressive neurodegenerative disorder characterized by insidious onset of memory loss, cognitive impairment, and gradual loss of functional independence, making it the most prevalent cause of dementia globally[1]. Epidemiological data suggest that over 55 million people are currently living with dementia, with AD contributing to approximately 60–70% of these cases[2][3][4]. Pathologically, AD is marked by extracellular amyloid-β (Aβ) plaque accumulation, intracellular tau protein hyperphosphorylation, and chronic neuroinflammation, which together drive synaptic dysfunction and neuronal loss[2][4][5]. Although our understanding of these mechanisms has deepened, early diagnosis remains difficult due to heterogeneous symptom onset, and effective disease-modifying therapies are still lacking.

Perioperative neurocognitive disorder (PND) is a collective term that encompasses cognitive impairments occurring in the perioperative period, including acute postoperative delirium and more persistent postoperative cognitive dysfunction[6]. PND is a major complication in elderly patients undergoing surgery, with an estimated 25% to 50% of older adults developing delirium after major procedures, and approximately 10% experiencing longer-lasting cognitive decline at three months postoperatively[7]. Intriguingly, PND and Alzheimer's disease (AD) share overlapping clinical features, such as memory loss and cognitive dysfunction. Moreover, the two conditions exhibit striking similarities in neuropathological mechanisms, including sustained neuroinflammation, blood–brain barrier disruption, and the accumulation of misfolded protein aggregates[7][8][9]. Epidemiological evidence further supports the association between PND and AD. In a prospective study of very elderly individuals without preexisting dementia, episodes of delirium were significantly associated with accelerated cognitive decline and a markedly increased risk of subsequent dementia[10][11][12]. Collectively, these

shared features, including inflammatory responses, vascular impairment, and proteopathic changes, raise the possibility that PND and AD may involve common molecular pathways. Consequently, perioperative molecular alterations associated with PND may serve as a valuable resource for identifying novel diagnostic biomarkers for Alzheimer's disease.

In this study, we integrated multi-cohort high-throughput transcriptomic data to systematically explore the molecular landscape of PND-related genes in the context of AD. By constructing a protein–protein interaction (PPI) network and applying machine learning algorithms, we prioritized a set of core PND-related genes associated with AD diagnosis, including RB1, PARK7, GLO1, ENO2, MDH2, and TUBB. Based on these biomarkers, we developed a nomogram model with high predictive performance. We further characterized functional pathway alterations and immune infiltration profiles related to these genes, and constructed a drug–target interaction network to highlight potential therapeutic opportunities. Finally, we performed in vivo validation in the 5×FAD mouse model to provide experimental support for the dysregulation trends of these candidate biomarkers.

2. Materials and methods

2.1 Public data sources acquisition and pre-process

The gene expression matrix and corresponding clinical data for Alzheimer's disease (AD) were retrieved from the Gene Expression Omnibus (GEO, https://www.ncbi.nlm.nih.gov/geo/). In this study, transcriptome microarray data of AD-affected hippocampal samples and their paired normal samples from GSE5281 were incorporated. Additionally, AD-affected hippocampal samples and their paired normal hippocampal samples from GSE48350 were utilized for validation. The "NormalizeBetweenArrays" function of the "limma" R package was employed to eliminate batch effects. Similar to the previously study [13], Perioperative neurocognitive disorder-related genes were downloaded from GeneCard (https://www.genecards.org).The overall research framework is presented in Figure 1.

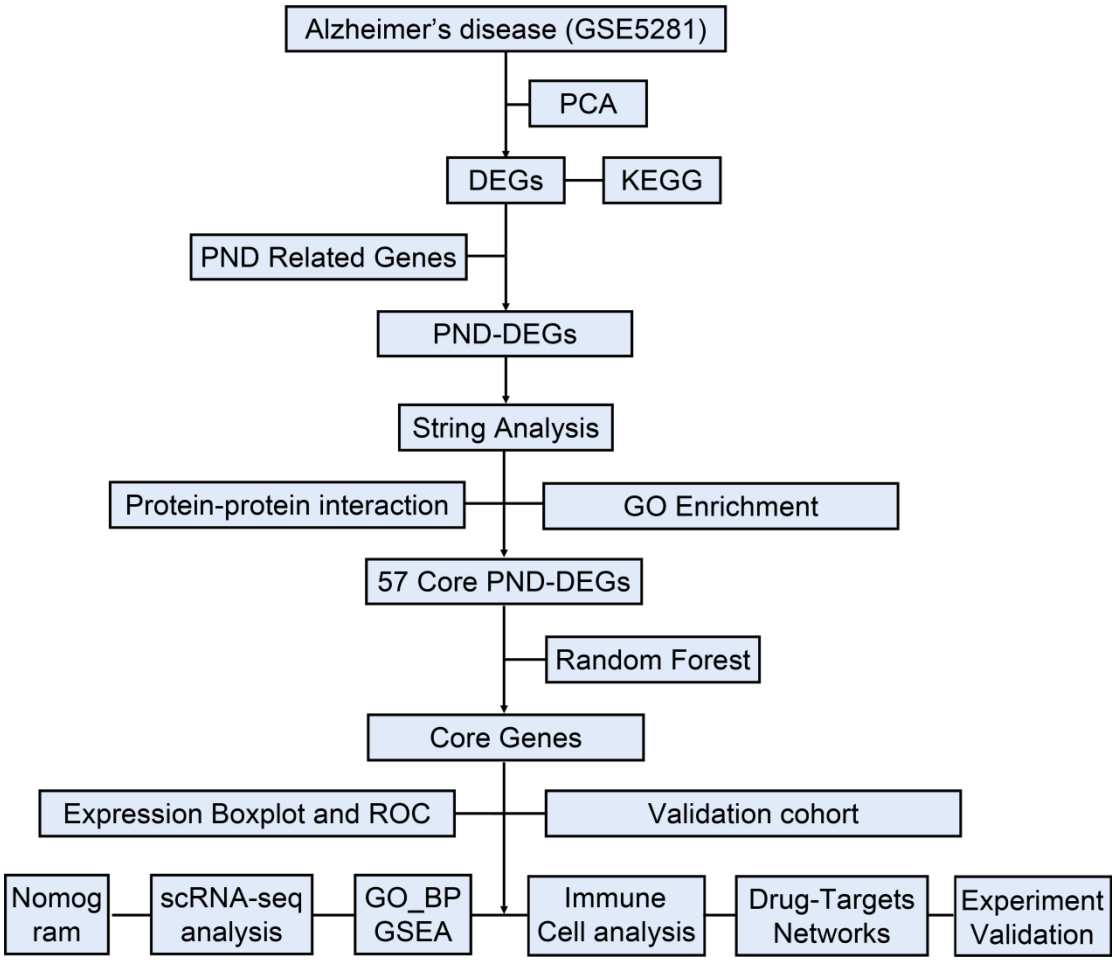


Figure 1. Research framework of this study

2.2 Differential expression genes analysis

To systematically identify differentially expressed genes (DEGs) between the disease group and the control group, we performed differential expression analysis using the "limma" package in R, which employs a linear modeling approach and empirical Bayes moderation for robust statistical inference[14]. Genes meeting the criteria of a p-value < 0.05 and a fold change threshold of |log2-FC| > 1 were defined as significantly differentially expressed. To clearly visualize the distribution and statistical significance of identified DEGs, we utilized the "genekitr" package in R to construct volcano plots, facilitating intuitive interpretation of the magnitude of gene expression changes and their corresponding statistical significance.

2.3 Pathway enrichment analysis

To explore the biological functions and signaling pathways associated with differentially expressed genes (DEGs), we conducted Gene Ontology (GO) and Kyoto Encyclopedia of Genes and Genomes (KEGG) pathway enrichment analyses using the "clusterProfiler" R package[15]. Results with significantly enriched terms (P.adjust < 0.05) were visualized using the "genekitr" R package[16]. Additionally, gene set enrichment analysis (GSEA) was performed to identify pathway enrichment in patients with varying levels of gene expression. GOBP pathways were utilized for GSEA, which was also conducted using the "genekitr" package. Enrichment results with P.adjust < 0.05 were considered statistically significant.

2.4 Protein-Protein Interaction Networks analysis

Proteins interact with each other to form functional networks, where theoretically, the more enriched the interactions, the more central the biological functions they represent. A total of 167 PND related differentially expressed genes (DEGs) of Alzheimer's disease were input into the STRING database to construct a protein-protein interaction (PPI) network. GOBP Pathway enrichment analysis was conducted using STRING (https://string-db.org), with no specific parameters predefined[17]. Based on the STRING analysis, a total of 57 proteins with a degree score greater than the average were identified as core proteins in this study and were included in subsequent analyses.

2.5 Identification of hub biomarkers using machine learning

To identify disease-specific feature genes using machine learning, we employed the "randomForest" R package to classify important genes through the Random Forest (RF) algorithm. RF analysis, based on a decision tree approach, identified the most significant variables (genes). A random forest model with 500 trees was constructed for the corresponding cohort, and the optimal number of trees was determined

by minimizing the cross-validation error. Genes were ranked by importance, and the top 10 most important genes were selected as feature genes for Alzheimer’s disease diagnosis.

2.6 scRNA-seq analysis

In this study, we employed ssREAD(https://bmblx.bmi.osumc.edu/ssread/), a comprehensive single - cell omics and spatial omics database for Alzheimer's disease (AD)[18]. Specifically we incorporated the disease samples (GSE185553) derived from the hippocampus of AD patients.

2.7 Immune infiltration analysis

The IOBR R package was used to estimate immune cells in the Alzheimer’s disease cohorts[19]. Specifically, the MPCounter algorithm was employed to quantify the relative immune cell fractions in individual samples. No specific parameters were manually set. t-test was used for statistical analysis of immune cell differences between groups, and Pearson correlation was applied to calculate correlations.

2.8 Construction of Drug-gene target network

For the analysis of the drug-target network, the DGIdb database was employed to identify the targets of relevant genes[20]. The DGIdb database, a comprehensive resource for drug-gene interactions, aggregates data from multiple sources. It not only offers information on known interactions between genes and drugs but also provides insights into potential associations. This includes data from preclinical research, clinical trials, and pharmacological databases. After retrieving and organizing the information on relevant targets and drugs from the DGIdb database, Cytoscape was utilized to construct the drug-target network[21].

2.9 Tissue collection and Quantitative RT-PCR

The 5×FAD mice expressing five familial AD gene mutations was commercially purchased and have been described previously[22]. All mice were maintained in the Animal Care Facility under ambient temperatures (26° ± 1°C), with a 12-hour light/12-hour dark cycle with unlimited access to standard rodent chow and clean water. All animal experiments were approved by the Institutional Animal Care and Use Committee at Qingdao University Medical School. Hippocampus tissue was harvested as described previously[23]. Six-month-old 5×FAD mice anesthetized by pentobarbital sodium via i.p. injection and cardiac perfused with saline. The hippocampus tissue was collected freshly and frozen immediately using liquid Nitrogen, and stored at −80 °C until use. Total RNA was extracted from hippocampus tissue with TRIzol reagent (Invitrogen, catalog no. 15596018). A 0.5 μg aliquot of total RNA was reverse-transcribed using a one-step first-strand cDNA synthesis kit (TransGen Biotech, catalog no. AT341). Quantitative real-time PCR (qRT-PCR) was performed with 2× SYBR Green PCR master mix (Genstars, catalog no. A304) on an Applied Biosystems QuantStudio 5 Real-time PCR System. The mRNA levels of target genes were quantified with comparative Ct method ($2^{-\Delta\Delta Ct}$) based on Ct values normalized to β-actin. Relevant Primers are provided in Table 1.

2.10 Statistical analysis

Data processing, analysis, and visualization were carried out using R packages (version 4.30; https://www.bioconductor.org/) or Graphpad Prism software (version 8.0.1; https://www.graphpad.com/). To compare differences between two groups, we employed Student's t-test. Correlation analysis between variables was performed using Pearson test. A significance level of $P < 0.05$ was considered statistically significant. Results are expressed as the mean ± standard error of the mean.

3. Results

3.1 Differential gene expression analysis reveals transcriptomic dysregulation and enriched pathways associated with Alzheimer’s disease

To explore the transcriptomic differences between Alzheimer’s disease (AD) and control groups, gene expression profiles were first normalized, resulting in consistent distributions across all samples. Boxplot visualization indicated consistent expression distributions across AD and control groups, supporting data comparability (Figure 2A). Principal component analysis (PCA) further illustrated a clear distinction between AD and control samples, suggesting significant transcriptomic differences reflective of disease-specific molecular signatures (Figure 2B). We next identified a total of 1,855 significantly differentially expressed genes (DEGs), comprising 958 upregulated and 897 downregulated genes in AD relative to control samples (Figure 2D). To explore expression patterns among these DEGs, hierarchical clustering analysis was performed, revealing distinct gene-expression profiles that effectively differentiated AD from control groups (Figure 2C). The observed transcriptional dysregulation emphasizes potential candidate biomarkers linked to AD pathology. Subsequent pathway enrichment analyses based on identified DEGs demonstrated significant enrichment of multiple biological pathways, particularly the PI3K－Akt signaling pathway, calcium signaling pathway, insulin secretion, and cGMP－PKG signaling pathway (Figure 2E). The involvement of these pathways suggests their potential roles in the pathophysiological mechanisms underlying Alzheimer’s disease.

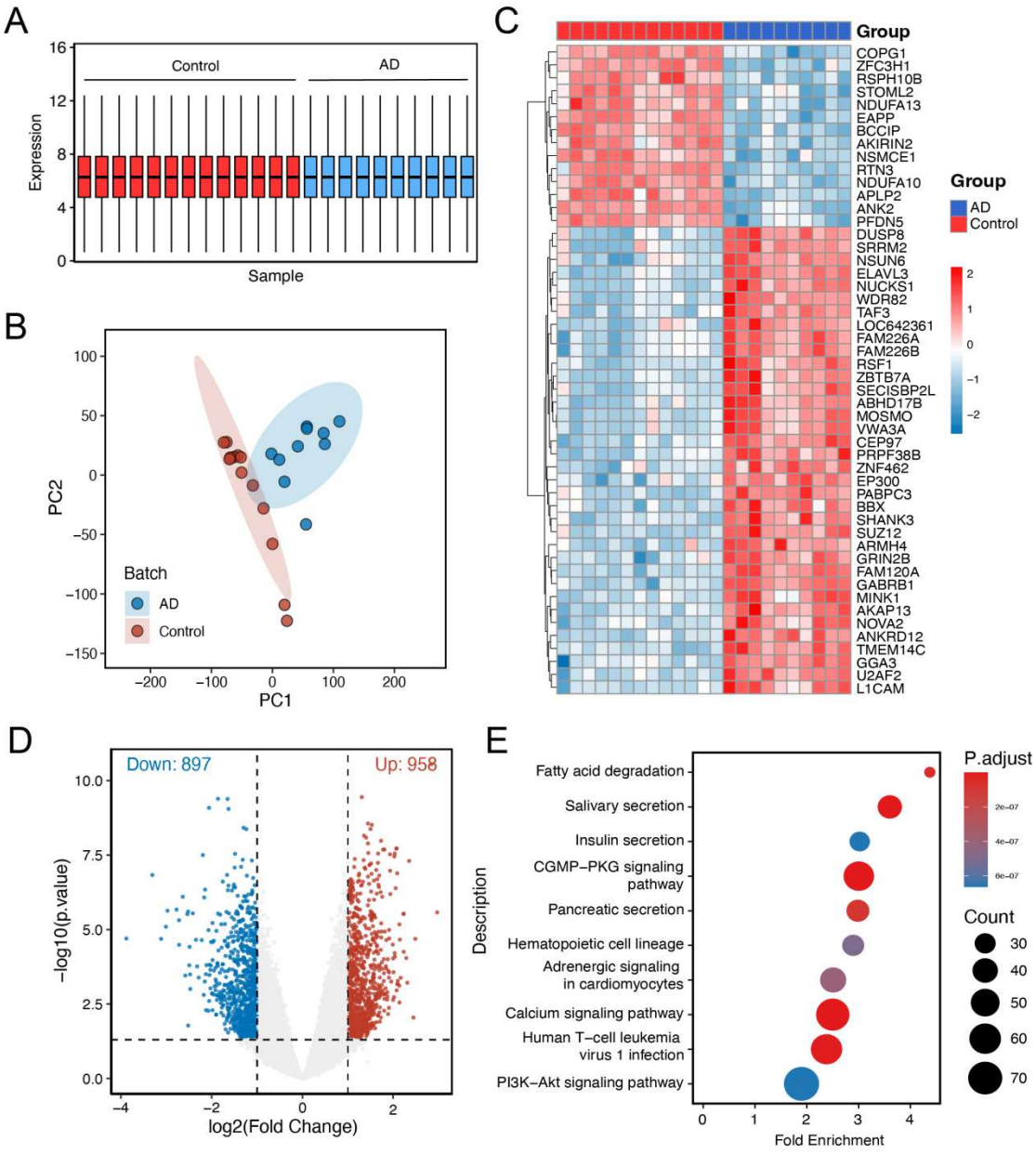


Figure 2. Differential gene expression analysis reveals transcriptomic dysregulation and enriched pathways associated with Alzheimer's disease

(A). Boxplot showing normalized expression levels across samples, indicating consistency and comparability of data distribution between AD and control groups. (B). Principal component analysis (PCA) plot illustrating the overall separation and clustering patterns of samples based on gene expression profiles. AD and control groups are clearly distinguishable, suggesting distinct transcriptional signatures. (C). Heatmap depicting hierarchical clustering of top significantly differentially expressed genes (DEGs)

between AD and control groups. Red represents upregulated expression, while blue indicates downregulated expression. Gene symbols are listed on the right. (D). Volcano plot summarizing DEGs identified with thresholds of p-value < 0.05 and |log2-FC| > 1. Red dots represent significantly upregulated genes (n = 958), blue dots represent significantly downregulated genes (n = 897), and grey dots indicate non-significant genes. (E). KEGG pathway enrichment analysis showing significantly enriched pathways based on DEGs. Dot size corresponds to gene counts within each pathway, and dot color indicates adjusted p-values.

3.2 Integrated bioinformatics analysis identifies perioperative neurocognitive disorder-related diagnostic biomarkers for Alzheimer's disease

Given the pathological associations reported between perioperative neurocognitive disorder (PND) and Alzheimer's disease (AD), the diagnostic potential of PND-associated genes in AD was further investigated. Initially, PND-associated genes were overlapped with differentially expressed genes (DEGs) identified in AD, resulting in a total of 167 intersecting candidate genes. Subsequently, a protein–protein interaction (PPI) network was constructed based on these overlapping genes to identify critical interacting proteins potentially relevant to AD (Figure 3A). Through PPI analysis, 57 hub proteins were identified, defined as those exhibiting interaction degrees equal to or greater than the network's average connectivity. Gene Ontology biological process (GO-BP) enrichment analysis was then conducted on these hub proteins, revealing significant enrichment in immune-related biological processes and signal transduction pathways, such as lymphocyte activation and regulation of the MAPK cascade (Figure 3B). These results suggest that dysregulation of immune cell function and key signaling pathways may play crucial roles in AD pathophysiology. To further identify core diagnostic biomarkers among these

candidate genes, a random forest algorithm was employed. A diagnostic model consisting of 500 decision trees was constructed, and gene importance scores were calculated to evaluate diagnostic efficacy (Figure 3C). Finally, the top 10 genes ranked by importance, including EP300, ANK2, PARK7, RB1, APP, CREBBP, MDH2, GLO1, ENO2 and TUBB, were selected as candidate biomarkers potentially valuable for AD diagnosis (Figure 3D).

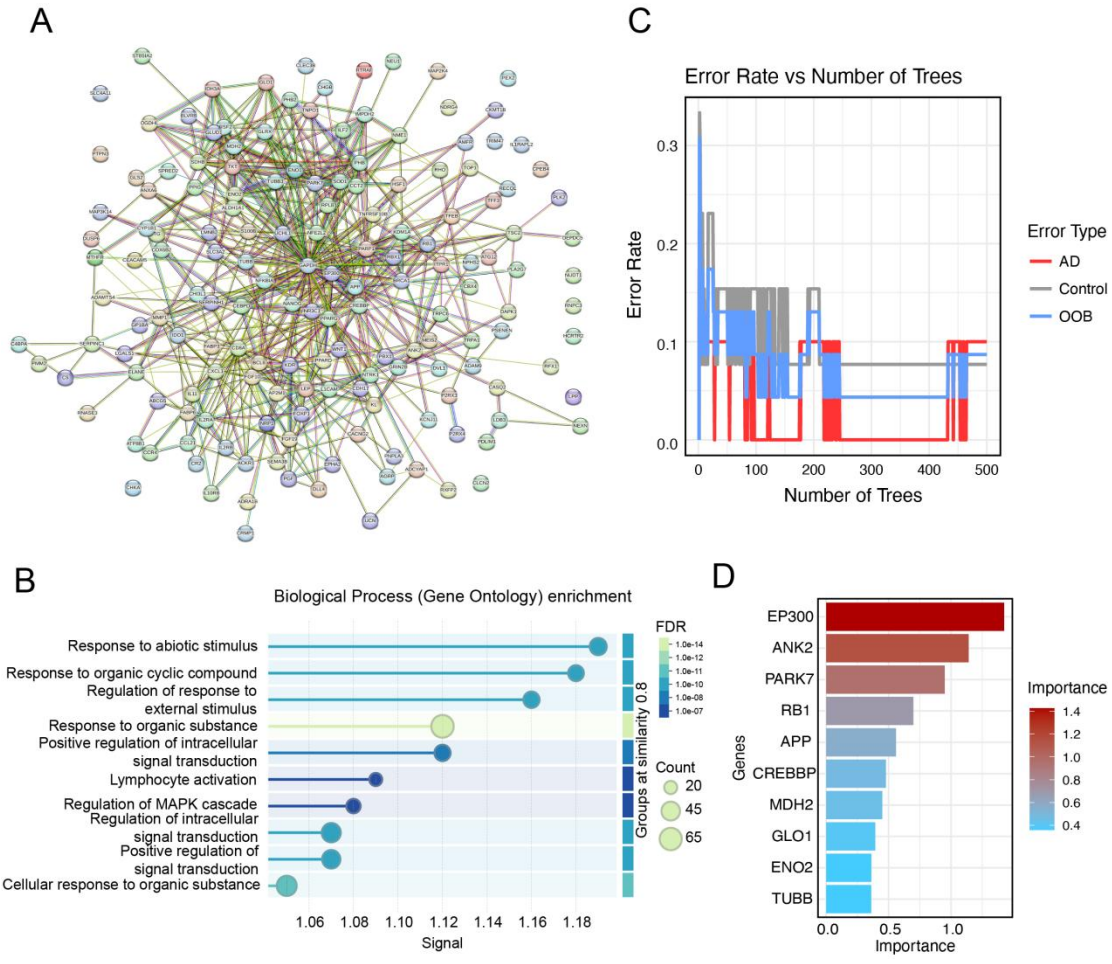


Figure 3. Integrated bioinformatics analysis identifies perioperative neurocognitive disorder-related diagnostic biomarkers for Alzheimer's disease

(A). Protein-protein interaction (PPI) network constructed from significantly differentially expressed genes (DEGs). (B). GOBP pathways enrichment dotplot of overlap genes. (C). Error rate plot of the

Random Forest diagnostic model constructed using the core proteins. (D). Feature importance barplot displaying the top 10 ranked candidate biomarkers identified from the Random Forest.

3.3 Validation of core perioperative neurocognitive disorder related diagnostic biomarkers for Alzheimer's disease

The differential expression patterns of ten identified candidate genes related to perioperative neurocognitive disorder (PND) were further validated between Alzheimer's disease (AD) and control groups using independent datasets. In the training cohort GSE5281, significantly elevated expression of EP300, RB1, APP, and CREBBP was observed in AD samples, suggesting that these genes might play a promotive role in AD pathology (Figure 4A). Moreover, genes including ANK2, PARK7, MDH2, GLO1, ENO2, and TUBB were significantly downregulated in AD samples compared to controls. Receiver operating characteristic (ROC) curve analyses further confirmed that these candidate genes exhibited excellent diagnostic performance, highlighting their potential as robust biomarkers (Figure 4B). In the additional validation cohort GSE48350, RB1 displayed significantly elevated expression in AD samples, consistent with results from the GSE5281 dataset (Figure 4C). Conversely, genes such as PARK7, MDH2, GLO1, ENO2, and TUBB remained significantly downregulated in AD samples. The ROC analysis conducted on the GSE48350 cohort reinforced the diagnostic significance of these genes (Figure 4D). Given the consistent differential expression trends of RB1, PARK7, MDH2, GLO1, ENO2, and TUBB across training and validation cohorts, these six genes were further confirmed as core PND-related AD diagnostic biomarkers. Finally, heatmap visualizations illustrated consistent expression patterns of these six core PND-related AD diagnostic biomarkers across individual samples in both

validation datasets (Figure 4E, F), providing further evidence supporting their robustness and reliability as diagnostic biomarkers for AD.

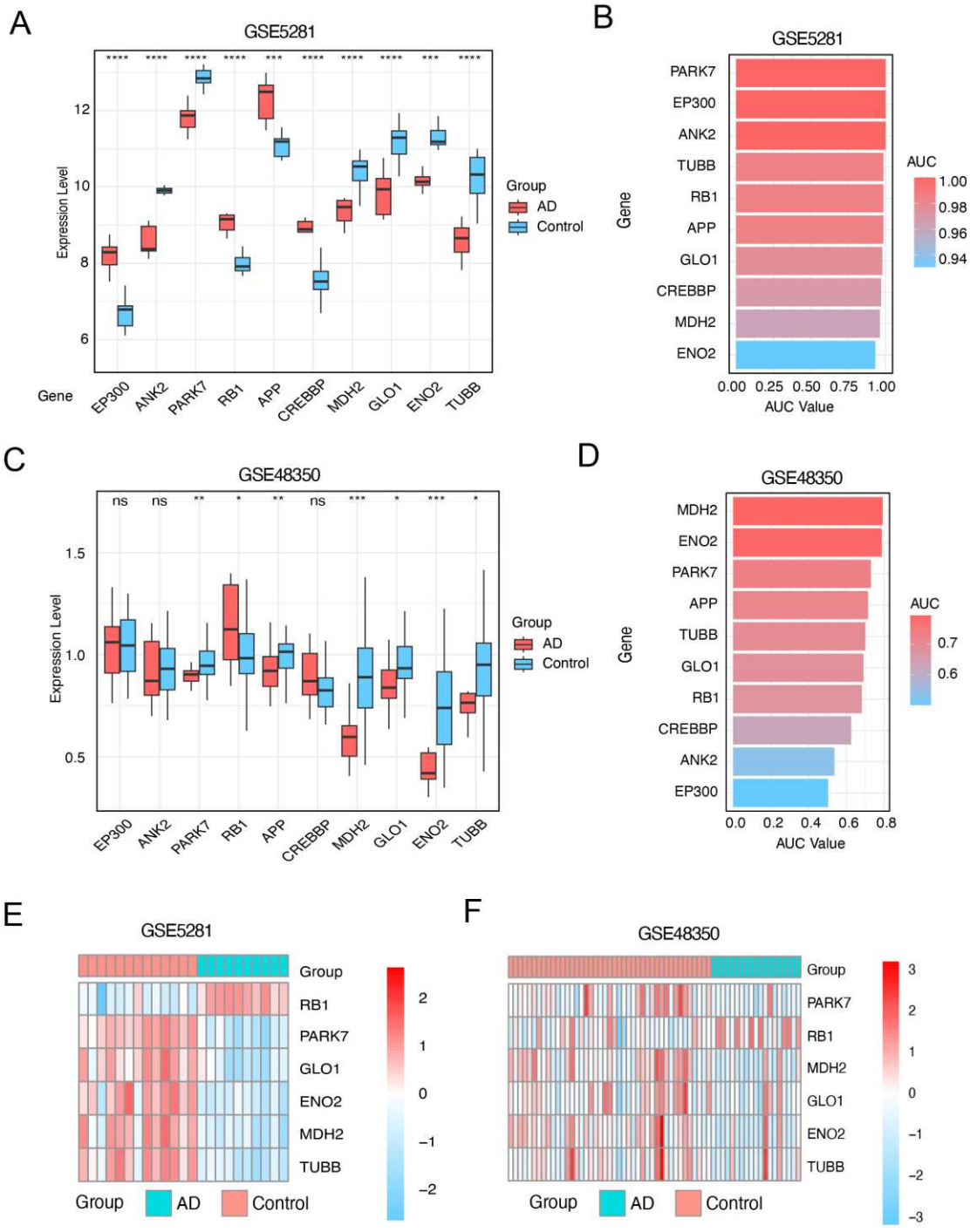
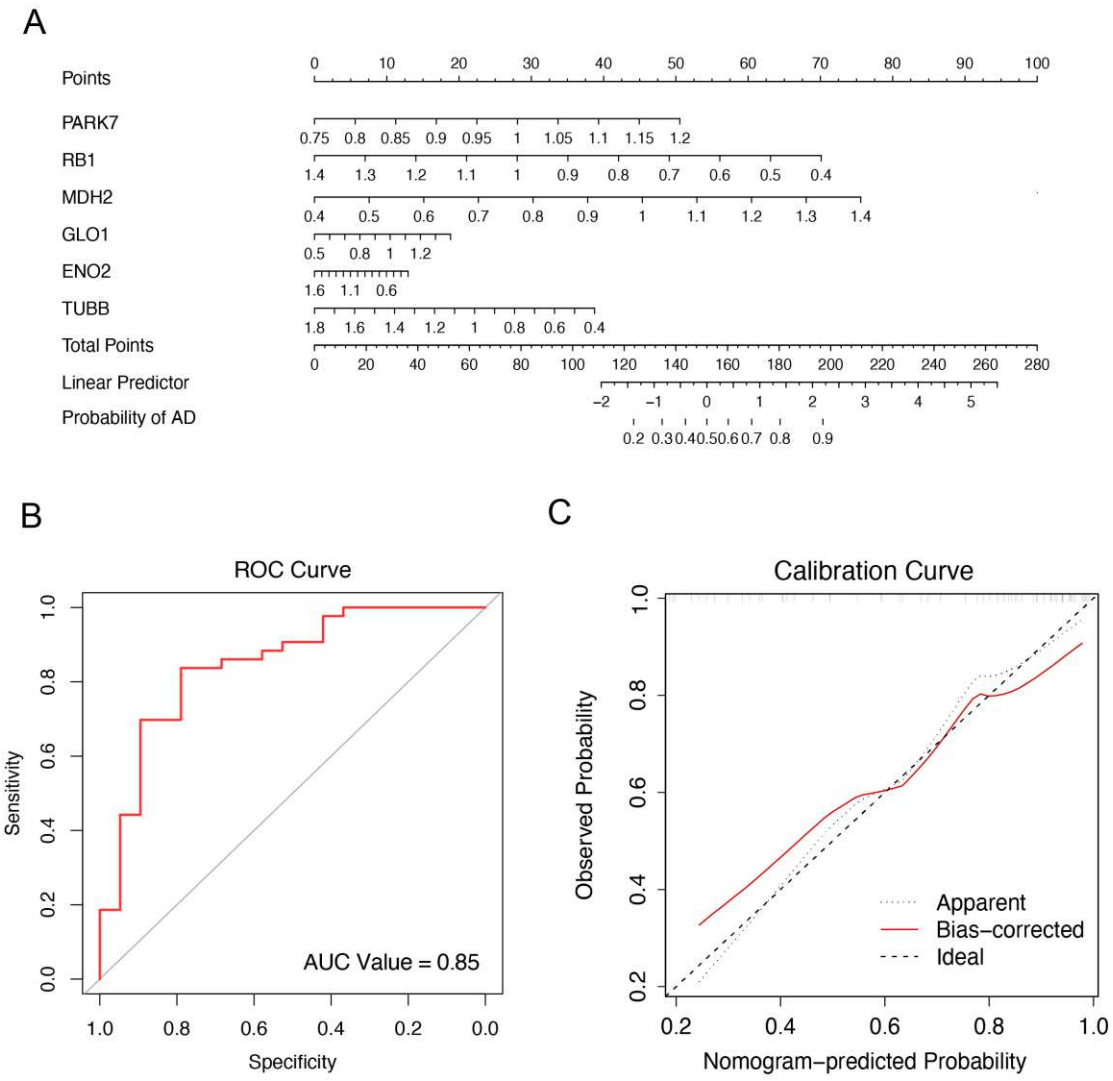


Figure 4. Validation of core perioperative neurocognitive disorder related diagnostic biomarkers for Alzheimer's disease

(A) . Boxplots illustrating the expression levels of the top 10 candidate diagnostic genes between AD and control groups in GSE5281. (B). Bar plots showing the diagnostic accuracy of each candidate gene measured by the area under the receiver operating characteristic curve (AUC) values in GSE5281. (C). Boxplots illustrating the expression levels of the top 10 candidate diagnostic genes between AD and control groups in GSE48350. (D). Bar plots showing the diagnostic accuracy of each candidate gene measured by the area under the receiver operating characteristic curve (AUC) values in GSE48350. (E). Heatmaps representing the relative expression patterns of the validated 6 core candidate genes across individual samples in GSE5281. (F). Heatmaps representing the relative expression patterns of the validated 6 core candidate genes across individual samples in GSE48350.

3.4 Construction a nomogram for Alzheimer's disease diagnosis

To further improve the diagnostic accuracy for Alzheimer's disease (AD), a nomogram incorporating six core perioperative neurocognitive disorder (PND)-related diagnostic biomarkers (PARK7, RB1, MDH2, GLO1, ENO2, and TUBB) was constructed (Figure 5A). In the validation cohort, the nomogram-based diagnostic model demonstrated excellent predictive performance, achieving an area under the receiver operating characteristic (ROC) curve (AUC) of 0.85, indicative of robust diagnostic capability (Figure 5B). Additionally, calibration curve analysis confirmed good agreement between the predicted probabilities and observed outcomes, suggesting the nomogram provides reliable yet conservative diagnostic predictions (Figure 5C). Taken together, these results suggest that the nomogram constructed from these six core genes has significant potential as a clinical diagnostic tool for AD.



272

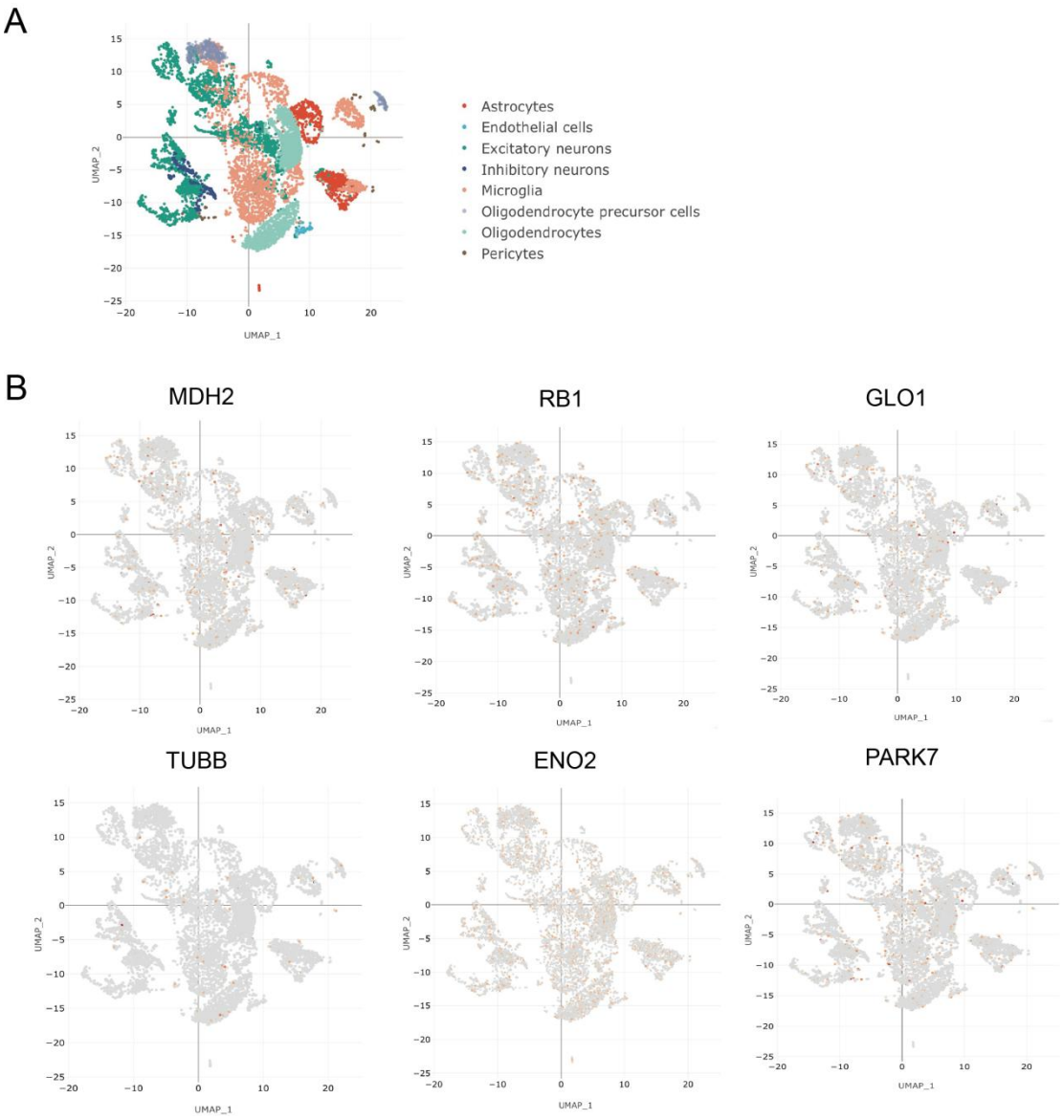
273 **Figure 5. Construction a nomogram for Alzheimer's disease diagnosis**

274 (A) . The nomogram integrating expression values of the six core diagnostic genes (PARK7, RB1, MDH2,
275 GLO1, ENO2, and TUBB). Each gene' s expression level corresponds to a specific point value. Total
276 points derived from individual gene scores are used to estimate the probability of Alzheimer' s disease.
277 (B). Receiver operating characteristic (ROC) curve of the overall diagnostic performance of the
278 nomogram. An area under the curve (AUC) of 0.85 indicates excellent discriminative ability in
279 differentiating AD patients from controls. (C). Calibration curve assessing the predictive accuracy of the
280 nomogram.

281

3.5 Single-cell analysis of core diagnostic genes

Cell types specific expression of six core diagnostic genes was further characterized. We analyzed single cell RNA-seq data derived from the hippocampus of Alzheimer's disease (AD) patients in GSE185553 using the ssREAD database. Cells were annotated into several cell subsets, including astrocytes, endothelial cells, excitatory neurons, inhibitory neurons, microglia, oligodendrocyte precursor cells, oligodendrocytes, and pericytes (Figure 6A). Feature plots of gene expression of the core diagnostic genes demonstrated non-cell specific expression patterns of the relevant genes. This finding implies the role of the genes mentioned above in the development and progression of AD across multiple cell types (Figure 6B).



291

292 **Figure 6. Single-cell analysis of core diagnostic genes**

293 (A) Cell-annotated UMAP plot of the hippocampal tissue in AD patients, with different colors
294 representing different cell types. (B) UMAP plot of single-cell expression of core diagnostic genes. The
295 red color represents cells with positive expression.

296

297 **3.6 Functional enrichment analysis of the six core perioperative neurocognitive disorder-related**
298 **Alzheimer's disease diagnostic genes.**

To further elucidate the biological roles of the six core perioperative neurocognitive disorder (PND)-related Alzheimer’s disease (AD) diagnostic genes (TUBB, ENO2, RB1, GLO1, PARK7, and MDH2), Gene Set Enrichment Analysis(GSEA) of gene ontology biological process(GOBP) was performed. Functional analysis of PARK7 highlighted its significant involvement in metabolic pathways and immune regulation, particularly carboxylic acid biosynthesis, adaptive immune response modulation, and negative regulation of immune cell activation (Figure 7A). The gene ontology analysis for MDH2 indicated its enrichment primarily in developmental and differentiation-related biological processes, such as myoblast differentiation, endochondral bone growth, and cell shape regulation, suggesting potential contributions to cellular morphology and neuronal differentiation abnormalities observed in AD (Figure 7B). For RB1, significant enrichment was observed in processes related to immune cell chemotaxis and differentiation, including leukocyte chemotaxis, lymphocyte chemotaxis, and the regulation of hematopoiesis. This further supports its involvement in immune activation or inflammation pathways implicated in AD pathology (Figure 7C). The enriched pathways for GLO1 included cellular biosynthetic processes and signaling pathways associated with gliogenesis, angiogenesis, and integrin-mediated signaling, suggesting potential roles in neurovascular remodeling and glial cell function in AD (Figure 7D). TUBB was significantly associated with metabolic processes, notably ATP metabolism, nucleoside triphosphate metabolic processes, and ribose phosphate metabolism, suggesting its potential role in energy homeostasis and cellular metabolism dysregulation in AD (Figure 7E). Lastly, activation of immune - related pathways exhibited a negative correlation with ENO2 expression. These immune - related processes include cellular responses to type I interferon, interferon - mediated signaling pathways, and general cellular defense responses. This finding highlights ENO2's potential role in immune dysregulation during the progression of Alzheimer's disease (Figure 7F). Collectively, these functional

enrichment analyses provide deeper insights into the potential biological mechanisms through which these core diagnostic genes may influence Alzheimer's disease pathology, especially emphasizing roles in immune modulation, metabolic dysfunction, and neuronal differentiation.

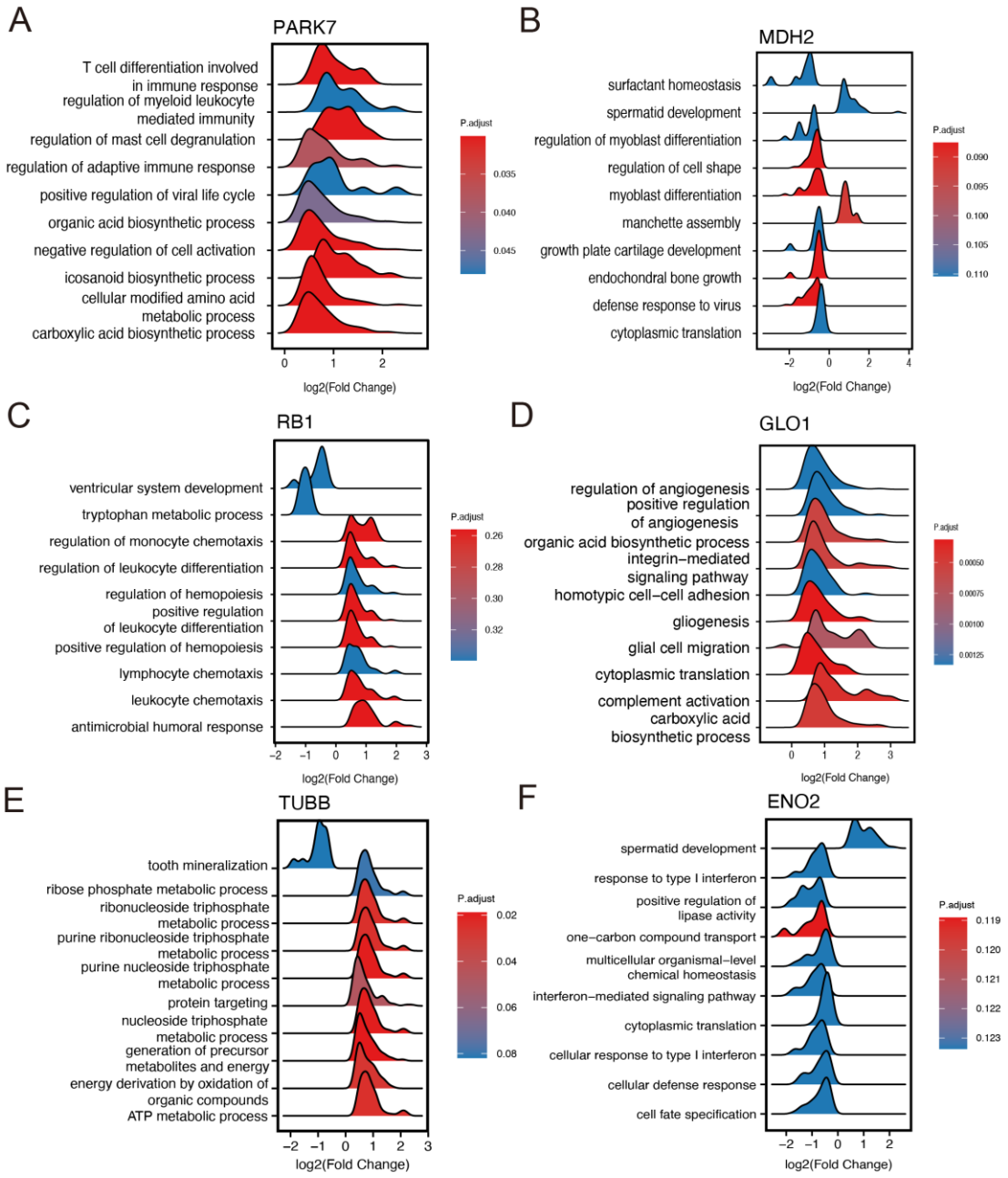


Figure 7. Functional enrichment analysis of the six core perioperative neurocognitive disorder-related Alzheimer's disease diagnostic genes.

(A-F). Ridge plots of Gene Set Enrichment Analysis (GSEA) of biological processes associated with PARK7, MDH2, RB1, GLO1, TUBB and ENO2 in Alzheimer's disease.

3.7 Immune infiltration analysis of Alzheimer's disease

Given immune-related pathways were identified as significantly associated with Alzheimer's disease (AD) mediated by perioperative neurocognitive disorder (PND)-related genes. Additionally, the progression of AD has been increasingly recognized to involve neuroinflammatory mechanisms. Thus, the association between these genes and immune cell populations was further investigated. Immune cell abundance level for each sample were estimated using the MPCounter deconvolution algorithm. Specifically, abundance level of T cells, CD8 T cells, Cytotoxic lymphocytes, B lineage, NK cells, Monocytic lineage, Myeloid dendritic cells, Neutrophils, Endothelial cells, and Fibroblasts were determined. Upon comparing immune cell abundance level between the AD and control groups in the discovery cohort, Monocyte lineage abundance was found to be significantly elevated in the AD group (Figure 8A). Previous studies have reported that under pathological conditions, monocytes infiltrate into the hippocampus, subsequently differentiating into pro-inflammatory cell lineages that promote neuro-inflammation. Consistent with these reports, our findings further suggest a pathological role for monocyte-associated immune cells in the progression of AD.

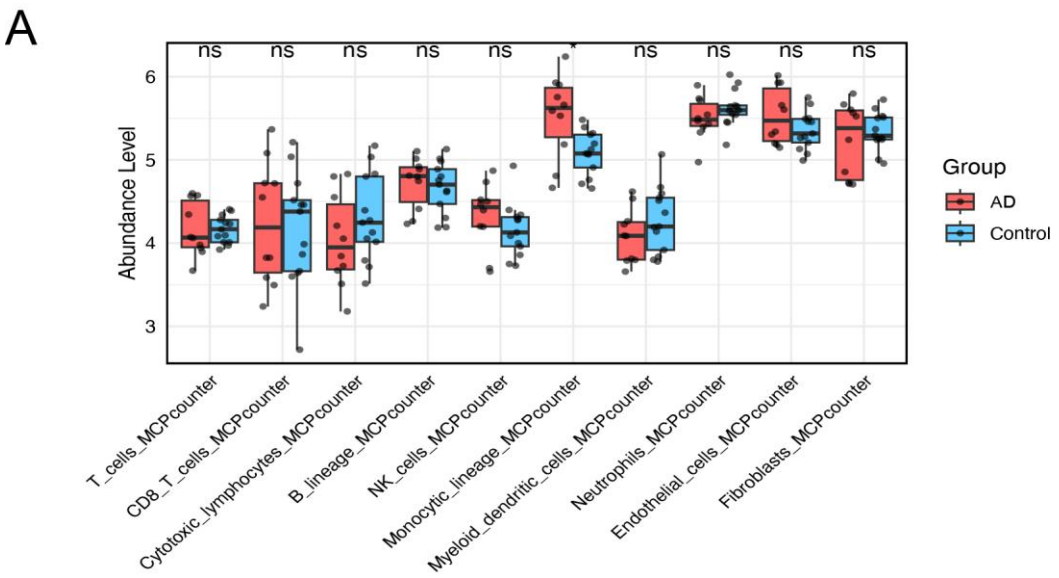


Figure 8. Immune infiltration analysis of Alzheimer's disease

(A) Boxplot of immune cell score in Alzheimer's disease and control groups. (*P<0.05).

3.8 Immune cell correlation analysis of the six core perioperative neurocognitive disorder-related Alzheimer's disease diagnostic genes

To further verify the association between core perioperative neurocognitive disorder (PND)-related Alzheimer's disease (AD) diagnostic biomarkers and immune cell infiltration, Pearson correlation analyses were conducted. For PARK7, negative correlations were identified with multiple immune cell fractions, particularly monocytic lineage cells, CD8 T cells, and NK cells, suggesting an inverse relationship with immune infiltration patterns (Figure 9A). MDH2 exhibited positive correlations predominantly with neutrophils and cytotoxic lymphocytes, whereas significant negative correlations were observed with endothelial and monocytic lineage cells (Figure 9B). Analysis of RB1 revealed significant positive associations with monocytic lineage, while negative correlations were detected with cytotoxic lymphocytes (Figure 9C). The correlation analysis of GLO1 indicated positive relationships

with cytotoxic lymphocytes and neutrophils, and negative associations with NK cells, CD8 T cells, and monocytic lineage cells (Figure 9D). Expression levels of TUBB showed significant positive correlations with neutrophils, whereas negative correlations were observed with CD8 T cells, monocytic lineage cells and endothelial cells (Figure 9E). Finally, ENO2 displayed negative correlations with monocytic lineage and endothelial cells, but positive correlations with neutrophils, cytotoxic lymphocytes (Figure 9F). Collectively, these results underscore significant correlations between the expression of core diagnostic biomarkers and immune cell abundance level, providing additional evidence of immune dysregulation as a critical pathological mechanism in Alzheimer's disease.

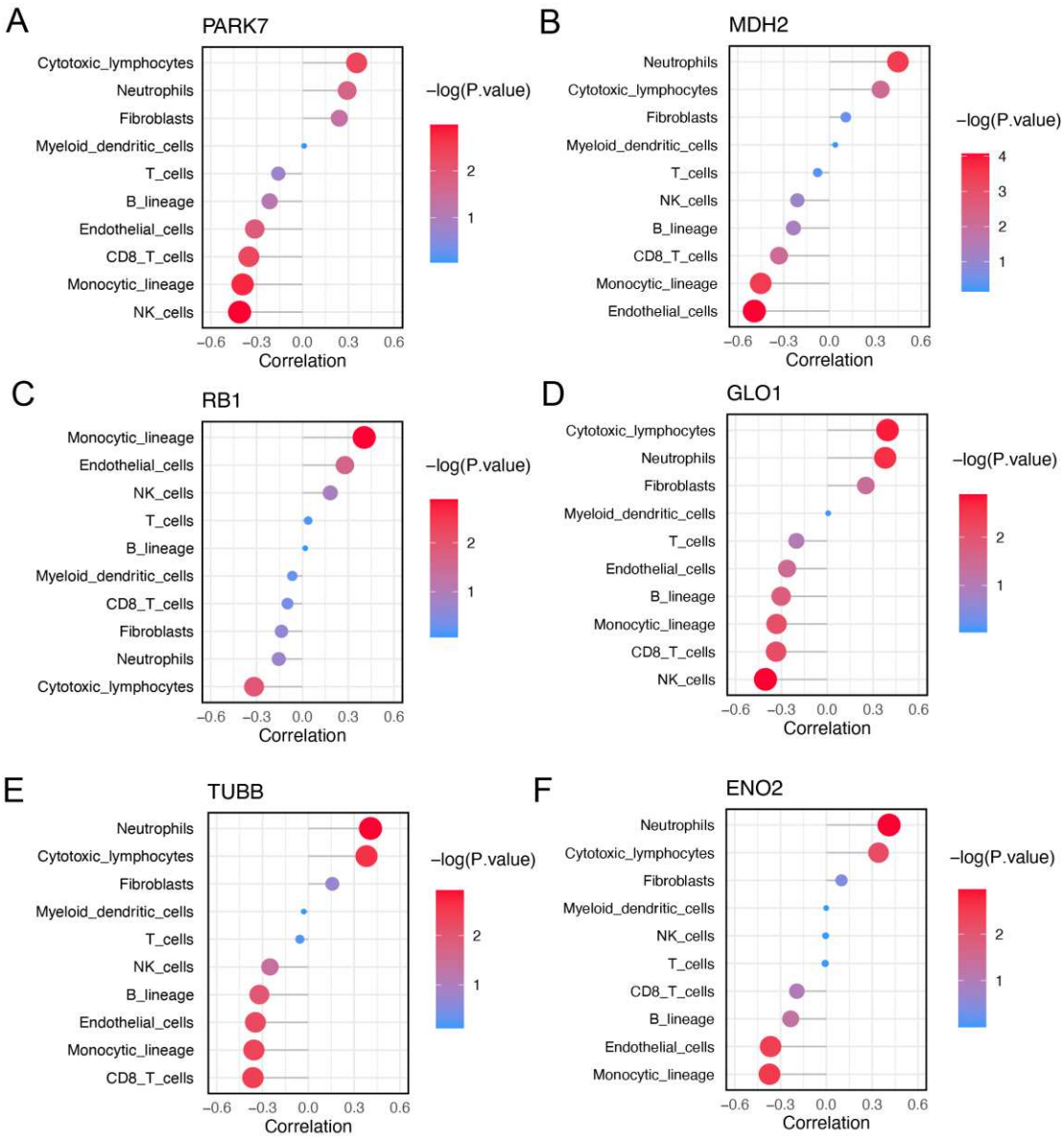
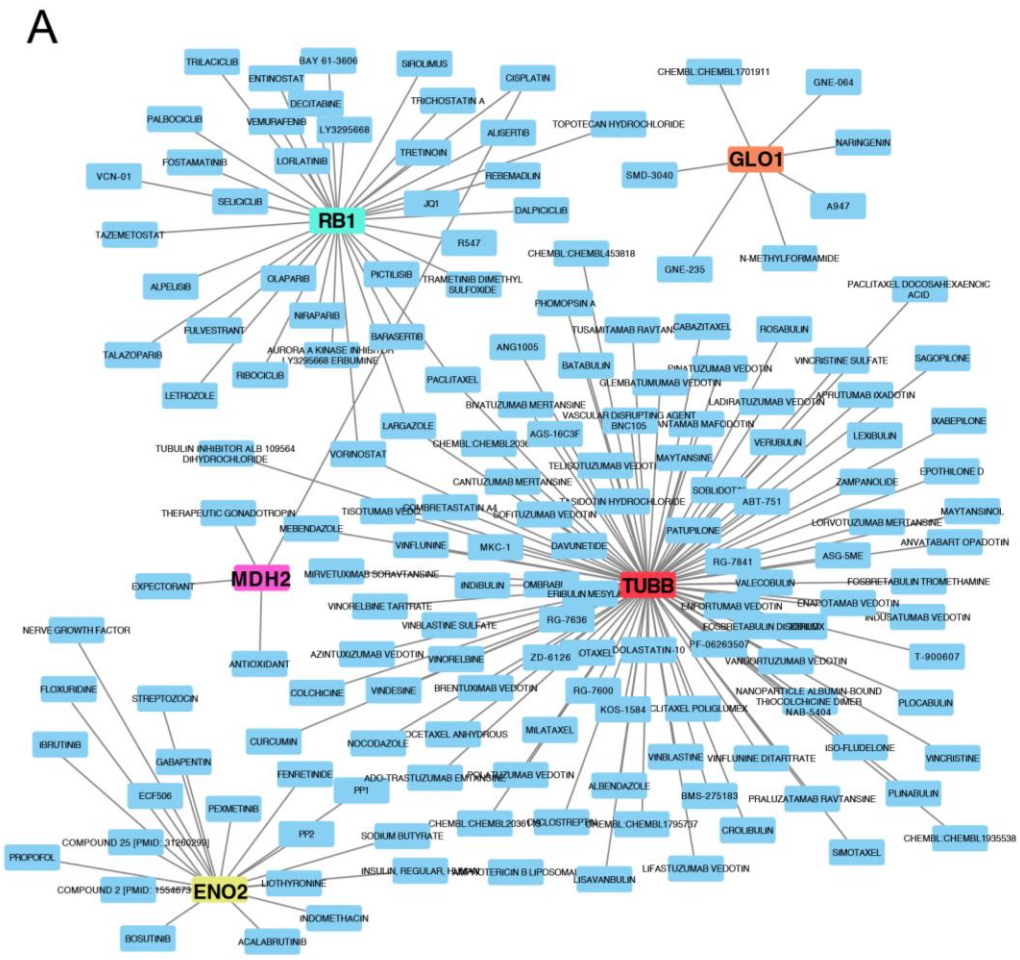


Figure 9. Immune cell correlation analysis of the six core perioperative neurocognitive disorder-related Alzheimer's disease diagnostic genes

(A-F) Pearson correlation Dot-plot between gene expression and immune cell abundance level. Correlation strength is represented by horizontal axis values; color intensity indicates statistical significance as expressed by -log(P-value).

3.9 Drug and gene targets network of core perioperative neurocognitive disorder-related Alzheimer’s disease diagnostic genes

Given the crucial role of perioperative neurocognitive disorder (PND)-related diagnostic genes in Alzheimer's disease (AD), we next explored potential drugs targeting the relevant gene products. A total of 167 potential targeted drugs were further identified. Specifically, this included 19 potential molecules targeting ENO2, 36 targeting RB1, 7 with GLO1 as a potential target, 4 targeting MDH2, and 99 targeting TUBB. Notably, our analysis indicated that TUBB - targeting drugs such as CURCUMIN, GLO1 - targeting drugs like NARINGENIN, and ENO2 - targeting drugs such as GABAPENTIN have demonstrated efficacy in improving preclinical AD models (Figure 10A). This finding validates the results of our analysis.



388

389 **Figure 10. Drug and gene targets network of core perioperative neurocognitive disorder-related**

390 **Alzheimer's disease diagnostic genes**

391 (A) Drug-gene target network. The blue nodes represent different drugs, and the nodes with gene names

392 marked in different colors are displayed.

393

394 **3.10 Experimental validation of six core perioperative neurocognitive disorder-related Alzheimer'**

395 **s disease diagnostic genes in the 5×FAD Alzheimer's disease mouse model**

To experimentally validate the expression patterns of the six core perioperative neurocognitive disorder (PND)-related Alzheimer’s disease (AD) diagnostic genes identified from transcriptomic analyses, we examined their expression levels in the brains of 5×FAD transgenic mice, a well-established AD model, and compared them with age-matched wild-type (WT) controls. RB1 expression was significantly increased in the brains of 5×FAD mice relative to WT controls. In contrast, PARK7, ENO2, and MDH2 showed significantly reduced expression in the 5×FAD group. GLO1 and TUBB also displayed a downward trend; however, these decreases did not reach statistical significance (Figure 11A). Overall, the expression changes observed in the 5×FAD model were largely concordant in direction with the differential expression patterns detected in the human AD transcriptomic datasets, supporting the cross-species reproducibility of these candidate biomarkers. Collectively, these in vivo results partially corroborate our bioinformatics-based identification of RB1, PARK7, GLO1, ENO2, MDH2, and TUBB as core PND-related diagnostic genes in AD and suggest their potential involvement in AD-associated molecular dysregulation.

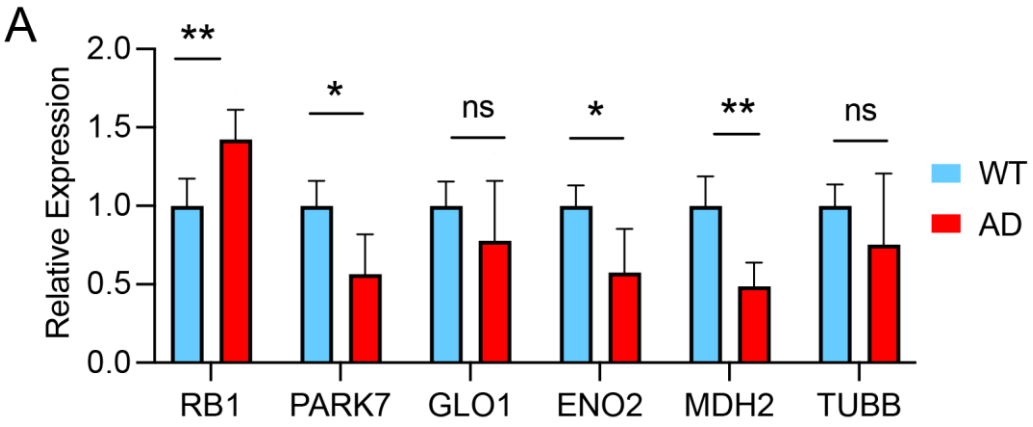


Figure 11. Experimental validation of six core perioperative neurocognitive disorder-related Alzheimer’s disease diagnostic genes in the 5×FAD Alzheimer’s disease mouse model

(A) Quantitative analysis of RB1, PARK7, GLO1, ENO2, MDH2 and TUBB mRNA expression levels via RT-qPCR. The panel compares 5FAD AD mouse model with WT.

4. Discussion

Perioperative neurocognitive disorder (PND), including acute postoperative delirium and long-term cognitive decline, shares key pathological features and risk factors with Alzheimer’s disease (AD)[9]. Neuroinflammation is a central mechanism in both, as surgical stress and anesthesia can induce CNS immune responses — such as microglial activation, cytokine release, and blood–brain barrier disruption—paralleling the chronic inflammation seen in AD[2][7][24]. Patients experiencing PND, especially delirium, often show AD-related pathology and face increased dementia risk[25][26]. These overlaps support exploring the molecular connection between PND and AD. Here, we systematically identified PND-associated genes dysregulated in AD to uncover shared mechanisms and potential diagnostic biomarkers.

Six genes previously linked to PND, including RB1, PARK7, GLO1, ENO2, MDH2, and TUBB, were identified as potential diagnostic biomarkers for AD through integrated bioinformatics and machine learning analyses. A diagnostic nomogram constructed based on these genes achieved an area under the curve (AUC) of 0.85, indicating strong predictive accuracy. In addition, we performed in vivo validation in the 5×FAD transgenic mouse model. Directionally concordant with the transcriptomic findings, RB1 was significantly upregulated in 5×FAD brains, whereas PARK7, ENO2, and MDH2 were significantly downregulated; GLO1 and TUBB also showed a downward trend but did not reach statistical significance. Together, these results suggest that the transcriptional alterations linked to PND may capture key pathological features of AD. Importantly, the biological functions of these genes align well with established mechanisms of neurodegeneration, supporting their relevance as candidate markers. RB1 is a key cell cycle regulator, and its dysregulation may contribute to aberrant cell cycle reentry in postmitotic neurons, a phenomenon observed in AD. PARK7 (DJ1), a known neuroprotective protein,

mitigates oxidative stress; its deficiency can lead to toxic protein accumulation and neuronal apoptosis. GLO1, which detoxifies reactive carbonyl compounds, is critical for preventing the buildup of advanced glycation end products (AGEs). Reduced GLO1 activity exacerbates oxidative and inflammatory stress in AD, while its early upregulation may reflect a compensatory response to shared metabolic disturbances in both PND and AD[27]. MDH2, a mitochondrial malate dehydrogenase, reflects energy metabolism dysfunction. Its downregulation, along with other TCA cycle enzymes, has been observed in AD brains, aligning with known bioenergetic deficits[25]. Similar mitochondrial stress may occur in PND, potentially linking MDH2 to both conditions. TUBB, encoding beta-tubulin, is essential for microtubule structure. Microtubule instability, driven by tau aggregation, is a key feature of AD, and beta-tubulin has been shown to co-aggregate in neurofibrillary tangles[28][29]. Its inclusion suggests that cytoskeletal damage—possibly stress-induced in PND—is also relevant to AD. Collectively, these six genes constitute a biologically plausible molecular signature of neurocognitive dysfunction, encompassing critical processes such as cell cycle regulation, redox homeostasis, metabolic integrity, and structural maintenance.

Beyond their diagnostic utility, our analyses also provide insights into the potential pathophysiological roles of these biomarkers. Functional enrichment of the AD-related genes associated with PND revealed their involvement in pathways related to immune response, metabolic regulation, and proteostasis. Further immune cell infiltration analysis confirmed significant correlations between these genes and immune cell populations, highlighting their relevance to neuroimmune processes. These findings align with the central role of immune dysregulation and inflammation in the pathogenesis of AD.

Notably, virtual drug screening and network analysis identified potential therapeutic compounds targeting RB1, GLO1, ENO2, MDH2, and TUBB. Several top-ranked candidate compounds possess anti-neuroinflammatory or neuroprotective properties, aligning with the biological functions of the target genes. For instance, curcumin, a TUBB modulator, has been reported to reduce soluble and insoluble amyloid-beta (Aβ) levels and plaque burden in Alzheimer's disease (AD) mouse models by inhibiting glycogen synthase kinase-3β (GSK-3β)-mediated phosphorylation of presenilin-1 (PS1), thereby reducing γ-secretase activity[30]. Similarly, naringenin, a GLO1 modulator, significantly decreases Aβ deposition, microglial and astrocytic activation, and pro-inflammatory cytokine levels in AD mouse models[31]. These findings validate the efficacy of our drug prediction methodology, warranting further investigation into promising AD therapeutic compounds. Furthermore, the convergence of pathways between perioperative neurocognitive disorders (PND) and AD suggests that therapies targeting neuroinflammation or oxidative stress may enhance both postoperative cognitive recovery and mitigate long-term neurodegeneration.

In conclusion, our study highlights the molecular commonalities between PND and AD. The six identified genes represent potential diagnostic biomarkers in AD and provide insights into the biological mechanisms linking acute cognitive dysfunction and chronic neurodegeneration. Further investigation of our biomarker-based model's diagnostic accuracy and the therapeutic candidates identified is necessary, with the ultimate goal of improving outcomes for patients at risk of AD.

Declarations

Ethics approval and consent to participate

Not applicable.

Consent for publication

All author consent the publication of this work.

Availability of data and materials

All of the sequencing data of this study were collected from GEO (https://www.ncbi.nlm.nih.gov/geo/), The corresponding data set is provided in the method. Code can be provided on reasonable request.

Competing interests

The authors declare that the research was conducted in the absence of any commercial or financial relationships that could be construed as a potential conflict of interest.

Funding

This work was supported by Natural Science Foundation of Shandong Province (ZR2023QC028).

Authors' contributions

Mingjuan Li designed the study. Mingjuan Li, Yuan Dong and Shipeng Shang performed the bioinformatic analysis. Zhaoliang Gu and Yuan Dong carried out the animal experimentst. Jing Wang and Xiaosa Chi wrote the manuscript. Anmu Xie and Aijie Liu revised the manuscript.

Acknowledgment

None.

References

[1]. Zhang J, Zhang Y, Wang J, Xia Y, Zhang J, Chen L, Recent advances in Alzheimer's disease: Mechanisms, clinical trials and new drug development strategies. Signal Transduct Target Ther 9 (2024) 211. https://doi.org/10.1038/s41392-024-01911-3.

[2]. Abdelnour C, Agosta F, Bozzali M, Fougère B, Iwata A, Nilforooshan R, et al. Perspectives and challenges in patient stratification in Alzheimer's disease. Alzheimers Res Ther 14 (2022) 112. https://doi.org/10.1186/s13195-022-01055-y.

[3]. Cataldi R, Sachdev PS, Chowdhary N, Seeher K, Bentvelzen A, Moorthy V, et al. A WHO blueprint for action to reshape dementia research. Nat Aging 3 (2023) 469-471. https://doi.org/10.1038/s43587-023-00381-6.

[4]. Cummings J. New approaches to symptomatic treatments for Alzheimer's disease. Mol Neurodegener 16 (2021) 2. https://doi.org/10.1186/s13024-021-00424-9.

[5]. Jack CR, Jr., Knopman DS, Jagust WJ, Petersen RC, Weiner MW, Aisen PS, et al. Tracking pathophysiological processes in Alzheimer's disease: an updated hypothetical model of dynamic biomarkers. Lancet Neurol 12 (2013) 207-216. https://doi.org/10.1016/s1474-4422(12)70291-0.

[6]. Evered L, Silbert B, Knopman DS, Scott DA, DeKosky ST, Rasmussen LS, et al. Recommendations for the nomenclature of cognitive change associated with anaesthesia and surgery-2018. Br J Anaesth 121 (2018) 1005-1012. https://doi.org/10.1016/j.bja.2017.11.087.

[7]. Subramaniyan S, Terrando N. Neuroinflammation and Perioperative Neurocognitive Disorders. Anesth Analg 128 (2019) 781-788. https://doi.org/10.1213/ane.0000000000004053.

[8]. Wan Y, Xu J, Meng F, Bao Y, Ge Y, Lobo N, et al. Cognitive decline following major surgery is associated with gliosis, β-amyloid accumulation, and τ phosphorylation in old mice. Crit Care Med 38 (2010) 2190-2198. https://doi.org/10.1097/CCM.0b013e3181f17bcb.

[9]. Wang P, Velagapudi R, Kong C, Rodriguiz RM, Wetsel WC, Yang T, et al. Neurovascular and immune mechanisms that regulate postoperative delirium superimposed on dementia. Alzheimers Dement 16 (2020) 734-749. https://doi.org/10.1002/alz.12064.

[10]. The American Geriatrics Society/National Institute on Aging Bedside-to-Bench Conference: Research Agenda on Delirium in Older Adults. J Am Geriatr Soc 63 (2015) 843-852. https://doi.org/10.1111/jgs.13406.

[11]. Davis DH, Muniz Terrera G, Keage H, Rahkonen T, Oinas M, Matthews FE, et al. Delirium is a strong risk factor for dementia in the oldest-old: a population-based cohort study. Brain 135 (2012) 2809-2816. https://doi.org/10.1093/brain/aws190.

[12]. Fong TG, Jones RN, Shi P, Marcantonio ER, Yap L, Rudolph JL, et al. Delirium accelerates cognitive decline in Alzheimer disease. Neurology 72 (2009) 1570-1575. https://doi.org/10.1212/WNL.0b013e3181a4129a.

[13]. Zhang W, Shi G, Wang H, Feng M, Gao X, Xie Q, et al. Molecular Mechanism of Xingnao Kaiqiao Pill for Perioperative Neurocognitive Disorder and Its Correlation With Immune and Inflammatory Signaling Pathways Based on Network Pharmacology and Molecular Docking. Front Aging Neurosci 14 (2022) 925072. https://doi.org/10.3389/fnagi.2022.925072.

[14]. Ritchie ME, Phipson B, Wu D, Hu Y, Law CW, Shi W, et al. limma powers differential expression analyses for RNA-sequencing and microarray studies. Nucleic Acids Res 43 (2015) e47. https://doi.org/10.1093/nar/gkv007.

563 [15]. Wu T, Hu E, Xu S, Chen M, Guo P, Dai Z, et al. clusterProfiler 4.0: A universal enrichment tool
564 for interpreting omics data. Innovation (Camb) 2 (2021) 100141.
565 https://doi.org/10.1016/j.xinn.2021.100141.
566 [16]. Liu Y, Li G. Empowering biologists to decode omics data: the Genekitr R package and web server.
567 BMC Bioinformatics 24 (2023) 214. https://doi.org/10.1186/s12859-023-05342-9.
568 [17]. Szklarczyk D, Gable AL, Lyon D, Junge A, Wyder S, Huerta-Cepas J, et al. STRING v11: protein-
569 protein association networks with increased coverage, supporting functional discovery in genome-wide
570 experimental datasets. Nucleic Acids Res 47 (2019) D607-D613. https://doi.org/10.1093/nar/gky1131.
571 [18]. Wang C, Acosta D, McNutt M, Bian J, Ma A, Fu H, et al. A single-cell and spatial RNA-seq
572 database for Alzheimer's disease (ssREAD). Nat Commun 15 (2024) 4710.
573 https://doi.org/10.1038/s41467-024-49133-z.
574 [19]. Zeng D, Ye Z, Shen R, Yu G, Wu J, Xiong Y, et al. IOBR: Multi-Omics Immuno-Oncology
575 Biological Research to Decode Tumor Microenvironment and Signatures. Front Immunol 12 (2021)
576 687975. https://doi.org/10.3389/fimmu.2021.687975.
577 [20]. Cannon M, Stevenson J, Stahl K, Basu R, Coffman A, Kiwala S, et al. DGIdb 5.0: rebuilding the
578 drug-gene interaction database for precision medicine and drug discovery platforms. Nucleic Acids Res
579 52 (2024) D1227-D1235. https://doi.org/10.1093/nar/gkad1040.
580 [21]. Saito R, Smoot ME, Ono K, Ruscheinski J, Wang PL, Lotia S, et al. A travel guide to Cytoscape
581 plugins. Nat Methods 9 (2012) 1069-1076. https://doi.org/10.1038/nmeth.2212.
582 [22]. Cheng J, Dong Y, Ma J, Pan R, Liao Y, Kong X, et al. Microglial Calhm2 regulates
583 neuroinflammation and contributes to Alzheimer's disease pathology. Sci Adv 7 (2021) eabe3600.
584 https://doi.org/10.1126/sciadv.abe3600.

585 [23]. Dong Y, Li S, Lu Y, Li X, Liao Y, Peng Z, et al. Stress-induced NLRP3 inflammasome activation
586 negatively regulates fear memory in mice. J Neuroinflammation 17 (2020) 205.
587 https://doi.org/10.1186/s12974-020-01842-0.
588 [24]. Pichet Binette A, Gaiteri C, Wennström M, Kumar A, Hristovska I, Spotorno N, et al. Proteomic
589 changes in Alzheimer's disease associated with progressive A β plaque and tau tangle pathologies. Nat
590 Neurosci 27 (2024) 1880-1891. https://doi.org/10.1038/s41593-024-01737-w.
591 [25]. Jia D, Wang F, Yu H. Systemic alterations of tricarboxylic acid cycle enzymes in Alzheimer's
592 disease. Front Neurosci 17 (2023) 1206688. https://doi.org/10.3389/fnins.2023.1206688.
593 [26]. Witlox J, Eurelings LS, de Jonghe JF, Kalisvaart KJ, Eikelenboom P, van Gool WA. Delirium in
594 elderly patients and the risk of postdischarge mortality, institutionalization, and dementia: a meta-
595 analysis. Jama 304 (2010) 443-451. https://doi.org/10.1001/jama.2010.1013.
596 [27]. Yang Z, Zhang W, Lu H, Cai S. Methylglyoxal in the Brain: From Glycolytic Metabolite to
597 Signalling Molecule. Molecules 27 (2022) 7905. https://doi.org/10.3390/molecules27227905.
598 [28]. Puig B, Ferrer I, Ludueña RF, Avila J. BetaII-tubulin and phospho-tau aggregates in Alzheimer's
599 disease and Pick's disease. J Alzheimers Dis 7 (2005) 213-220; discussion 255-262.
600 https://doi.org/10.3233/jad-2005-7303.
601 [29]. Cyske Z, Gaffke L, Pierzynowska K, Węgrzyn G. Tubulin Cytoskeleton in Neurodegenerative
602 Diseases-not Only Primary Tubulinopathies. Cell Mol Neurobiol 43 (2023) 1867-1884.
603 https://doi.org/10.1007/s10571-022-01304-6.
604 [30]. Zang WB, Wei HL, Zhang WW, Ma W, Li J, Yao Y. Curcumin hybrid molecules for the treatment
605 of Alzheimer's disease: Structure and pharmacological activities. Eur J Med Chem 265 (2024) 116070.
606 https://doi.org/10.1016/j.ejmech.2023.116070.

607 [31]. Zhu Y, Guo X, Li S, Wu Y, Zhu F, Qin C, et al. Naringenin ameliorates amyloid-β pathology and
608 neuroinflammation in Alzheimer's disease. Commun Biol 7 (2024) 912. https://doi.org/10.1038/s42003-
609 024-06615-6.
610
611
612
613
614
615
616
617
618
619
620
621
622
623
624

625 **Table captions**

626 Table 1. Primers and the sequences applied in this study.

Supplementary Files

This is a list of supplementary files associated with this preprint. Click to download.

- Table1.xlsx